Nonrigid Registration with Adaptive, Content-Based Filtering of the Deformation Field

Marius Staring*, Stefan Klein and Josien P.W. Pluim

Image Sciences Institute, University Medical Center Utrecht, P.O. Box 85500, 3508 GA, Room Q0S.459, Utrecht, The Netherlands

ABSTRACT

In present-day medical practice it is often necessary to nonrigidly align image data, either intra- or inter-patient. Current registration algorithms usually do not take different tissue types into account. A problem that might occur with these algorithms is that rigid tissue, like bone, also deforms elastically. We propose a method to correct a deformation field, that is calculated with a nonrigid registration algorithm. The correction is based on a second feature image, which represents the tissue stiffness. The amount of smoothing of the deformation field is related to this stiffness coefficient. By filtering the deformation field on rigid tissue, the deformation field will represent a local rigid transformation. Other parts of the image containing nonrigid tissue are smoothed less, which leaves the original elastic deformation (almost) untouched. It is shown on a synthetic example and on inspiration-expiration CT data of the thorax, that a filtering of the deformation field based on tissue type indeed keeps rigid tissue rigid, thus improving the registration results.

Keywords: nonrigid registration, deformation field regularisation, deformation model

1. INTRODUCTION

Image registration is a common necessity in the clinic. A commonly used approach is to initially perform a rigid or affine registration to capture the global deformation, followed by a nonrigid registration step. In the latter step the whole volume is usually treated as nonrigid tissue. The output of a registration procedure is a deformation field, which when applied to the moving image results in the deformed image one is interested in. A popular example of such a nonrigid registration algorithm is the one described by Rueckert et al.[1]

A problem with this approach is that in the nonrigid step rigid structures, such as bones, are also treated nonrigidly. The rigidity of different tissue types is not taken into account. In this article we propose a method to nonrigidly register images, yet providing local rigid transformations within the deformation field, corresponding to rigid structures. This is achieved by an adaptive filtering of the deformation field.

Filtering has been used before on deformation fields, typically in optical flow like registration algorithms. Thirion[2] uses a Gaussian smoothing of the deformation fields as a regularisation to get more plausible results. He uses a fixed standard deviation σ for the Gaussian distribution for the whole deformation field. Cachier et al.[3] derive *a priori* and *a posteriori* smoothing weights for the Demons algorithm, with which they filter the deformation field. A different method to smooth the deformation field is used by Stefanescu et al.[4] They regularise the deformation field by smoothing it with a Gaussian $N(0, \sigma_i^2)$ with variance σ_i^2 depending on the voxel position. They propose to take large values in areas where little deformation is expected, and vice versa. Edwards et al.[5] model the deformation field by a physical representation based on finite elements. A three-component deformation model is used, consisting of rigid, elastic and fluid structures. Another way of restricting the deformation field is by incorporating an incompressibility constraint, like Rohlfing et al.[6] do by penalising a deviation of the Jacobian from 1. However, the latter method does not distinguish between different tissue types, and also does not enforce rigidity of stiff tissue.

We extend the filtering of the deformation field, by adaptive filtering based on tissue type. Different parts of the deformation field are filtered differently, based on the rigidity or stiffness of the tissue at hand. In this way stiff tissue is kept rigid, while nonrigid tissue is allowed to deform freely.

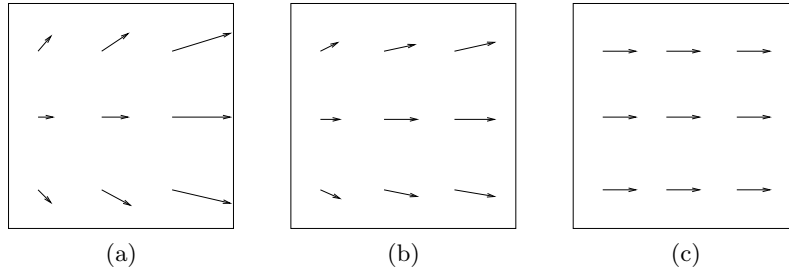*e-mail: `marius@isi.uu.nl`, telephone: +31 30 250 3186

Figure 1. The original 2D deformation field 1(a), stretches the underlying tissue both vertically and horizontally. Applying the adaptive filter once to this field results in 1(b). This field still stretches tissue, but less. After applying the adaptive filter many times, the result is a homogeneous deformation field 1(c), yielding a rigid transformation of the underlying tissue.

In Section 2 the proposed filter for regularising the deformation field is described in detail and an overview of the proposed registration algorithm is given. Details about the data used for validation are given in Section 3. The validation of the algorithm is described in Section 4, and the paper is concluded with a discussion in Section 5.

2. METHOD

Registration can be described as the problem of finding the deformation field that maps a moving image onto a fixed image. Let $A(x) : \mathbb{R}^D \mapsto \mathbb{R}$ denote the fixed image, where $x = (x_1, \ldots, x_D)$ is a voxel from an image of dimension D. Let $B(x) : \mathbb{R}^D \mapsto \mathbb{R}$ be the moving image. The registration algorithm returns a deformation field $d(x) : \mathbb{R}^D \mapsto \mathbb{R}^D$ from A to B, which yields the deformed image $C(x) = B(x + d(x))$. We propose to filter the deformation field $d(x)$ adaptively, based on the content of a 'stiffness coefficient' image $c(x)$.

The design of this filter is described in Section 2.1, the creation of the stiffness coefficient image $c(x)$ in Section 2.2. Finally, in Section 2.3 an overview of the proposed registration algorithm is given.

2.1. Filter design

The filtered deformation field $\tilde{d}(x) : \mathbb{R}^D \mapsto \mathbb{R}^D$ is constructed as follows. For each point x_i in the deformation field $d(x)$, a weighted mean $\mu(x)$ is calculated over a neighbourhood $\mathcal{N}_i$ of x_i

$$\mu(x_i; c, d) \triangleq \sum_{j \in \mathcal{N}_i} c(x_j) d(x_j) / \sum_{j \in \mathcal{N}_i} c(x_j). \tag{1}$$

This filter has a different shape at every spatial location, based on $c(x)$. Then, the updated deformation field $\tilde{d}(x)$ is defined by

$$\tilde{d}(x_i; c, \mu, d) \triangleq (1 - c(x_i)) d(x_i) + c(x_i) \mu(x_i), \quad \forall i, \tag{2}$$

where $c(x_i)$ should be between 0 and 1.

Consequently, a value close to the mean deformation $\mu(x)$ is assigned to $\tilde{d}(x)$ if the stiffness coefficient $c(x)$ is high, and a value close to the original deformation $d(x)$ for low stiffness coefficients. So, for stiff tissue, a weighted mean filtering is performed, which results in a smoothing of the deformation field. The result is a more homogeneous deformation field where $c(x)$ is high, that is where tissue is more stiff.

The adaptive filter can be applied to the deformation field several times in succession. This way both the power and the extent of the adaptive filter are increased. This effect is shown in Figure 1. Applying the filter more than once yields a smoother deformation field; the orientation and magnitude of the vectors in the neighbourhood become more similar. Also the size of the neighbourhood where this effect is noticeable is extended.

It is interesting to note that the adaptive filtering of the deformation field described above is related to the anisotropic diffusion framework.[7] Smoothing the deformation field with a Gaussian has been shown[8] to be equivalent to the linear diffusion equation

$$\frac{\partial}{\partial s} d(x, s) = c_0 \nabla^2 d(x, s), \tag{3}$$

with homogeneous diffusivity c_0, independent of the position x. In general form the diffusion equation can be written as

$$\frac{\partial}{\partial s} d(x, s) = \nabla \cdot (c(x, s) \nabla d(x, s)) = c(x, s) \nabla^2 d(x, s) + \nabla c(x, s) \nabla d(x, s). \tag{4}$$

Our adaptive filter, described in Equations (1) and (2), filters the deformation field based on the local stiffness coefficient $c(x)$. This is related to diffusion of the deformation field described by Equation (4) with non-homogeneous diffusivity $c(x)$. The amount of diffusion of the deformation field depends in this case on the diffusivity image $c(x)$ and on the time parameter s. This time parameter can be related to the repeated application of the adaptive filter. The work of Stefanescu et al. does not fit in the latter framework, since the derivative of c, ∇c, is not taken into account.

2.2. Stiffness coefficient

The stiffness coefficient image can be obtained by processing the fixed image, for example by segmenting the relevant structures and assigning a stiffness coefficient (a value within $[0, 1]$) to these structures.

2.3. Overview of the algorithm

The registration framework in which the proposed adaptive filtering method is incorporated, is described in this section. The algorithm is largely based on the papers of Rueckert et al.[1] and Mattes et al.[9] The methods described by these authors use the well-known mutual information as a similarity measure between the fixed and moving image. The deformation field is parameterised by cubic B-splines:

$$d(x) = d^{\text{BS}}(x; p^{\text{BS}}). \tag{5}$$

The set of B-spline coefficients $\{p^{\text{BS}}\}$ that maximise the mutual information is found using an iterative optimiser:

$$p_{t+1}^{\text{BS}} = p_t^{\text{BS}} + \Delta_t^{\text{BS}}, \tag{6}$$

where Δ_t^{BS} is a vector containing the B-spline parameter updates in iteration t. These updates depend on the derivative of the mutual information with respect to p_t^{BS}. Instead of optimising over B-spline parameters one can also optimise over deformation fields by rewriting Equations (5) and (6) to

$$d_{t+1}(x) = d_t(x) + d^{\text{BS}}(x; \Delta_t^{\text{BS}}). \tag{7}$$

In this manner, the description of the deformation field $d_t(x)$ at iteration t is decoupled from the description of the updated deformation field $d^{\text{BS}}(x; p_t^{\text{BS}})$. For standard B-spline based registration both deformation fields are described by B-splines. However, the decoupling makes it possible to represent each by a different parameterisation, resulting in more freedom to model the deformation.

Incorporating our adaptive filtering of the deformation field in the registration framework is straightforward:

$$d_{t+1}(x) = \mathcal{F} \left(d_t(x) + d^{\text{BS}}(x; \Delta_t^{\text{BS}}) \right), \tag{8}$$

where $\mathcal{F}(d)$ represents the adaptive filtering of a deformation field d. Hence, the deformation $d_t(x)$ is modelled by a filtered version of a B-spline based deformation field and does not fit anymore within a B-spline parameterisation of a deformation field. Only the updated field $d^{\text{BS}}(x; \Delta_t^{\text{BS}})$ is modelled by B-splines. This has fewer restrictions than modelling the entire transformation with B-splines. Combinations of rigid and nonrigid components in the transformation do not fit into the latter model. Our model provides more liberty in this respect.

First experiments have shown that it is not necessary to perform the adaptive filtering $\mathcal{F}$, described in Section 2.1, every iteration. Instead, the adaptive filtering is performed every n iterations. It is then applied several times (k) in succession. This way a more pronounced result can be obtained, as discussed in Section 2.1.

In order to calculate the updated B-spline parameters Δ_t^{BS} we use a stochastic gradient descent optimiser, which uses an approximation of the derivative of the mutual information with respect to the B-spline parameters p^{BS}.[10] To calculate the derivative of the similarity measure not all samples in the image are used, because this has been shown to accelerate registration significantly, without compromising registration accuracy.[10] Calculation of the mutual information is based on an implementation of Thévenaz and Unser.[11] In order to avoid local minima a multiresolution approach is taken.[12] A Gaussian image pyramid is used with a subsampling factor of 2. Also a multigrid approach is taken: when the image resolution is doubled, the B-spline control point spacing is halved. Prior to the nonrigid registration an affine registration is performed, in order to capture the global transformation between fixed and moving image.

Summarising, the proposed nonrigid registration is given by

1. Do n iterations of the optimiser, resulting in updated B-spline parameters $\{\Delta_t^{\mathrm{BS}}\}$, and in a new additional deformation field $d^{\mathrm{BS}}(x; \Delta_t^{\mathrm{BS}})$.

2. Calculate the deformation field $\hat{d}_{t+1}(x) = d_t(x) + d^{\mathrm{BS}}(x; \Delta_t^{\mathrm{BS}})$.

3. Filter the deformation field, i.e., calculate $d_{t+1}(x) = \mathcal{F}\left(\hat{d}_{t+1}(x)\right)$ according to Equations (1) and (2). Perform this step k times.

Repeat these four steps until the maximum amount of iterations is reached, and for all resolutions.

3. 3D CT DATA

Registration is performed on CT data of the thorax, acquired with a Philips 16 slice spiral CT scanner (Mx8000 IDT) using a high radiation dose. Scans of patients were made in the inspiration phase and in the expiration phase of respiration. Matching these intra-patient inspiration - expiration data is necessary in order to visualise changes such as airtrapping in the lungs and it could possibly provide a local perfusion map of the lungs.

We have four data sets available with slices of size 512×512 voxels. Each data set contains 300 - 400 slices, where the inspiration data set always has more slices than the expiration data. In-plane voxels are squared with sizes around 0.6×0.6 mm. Slice thickness is always 0.7 mm. Before registration each data set is downsampled with a factor of 2 in each dimension in order to reduce computer memory and computational load. Downsampling is performed by discarding odd rows, columns and slices. The inspiration data set is used as the fixed image and the expiration data as the moving image.

In Figure 2 two coronal slices of the CT data are shown. The inspiration data show substantially more lung volume. Registration based on B-splines will try to stretch the lungs from the expiration data to get a maximal overlap with the inspiration data. This will most likely result in stretching of the ribs in the vertical direction.

4. RESULTS

In order to evaluate the effectiveness of the proposed registration with adaptive filtering of the deformation field, it is compared with registration based only on B-splines. Both methods are described in Section 2.3. We first give an illustration of the two methods on synthetic images. We then compare them on clinical data, viz. the 3D CT inspiration - expiration data described in Section 3.

In all experiments with the adaptive filtering of the deformation field, the size of the neighbourhood $\mathcal{N}_i$ from Equation (1) is $3 \times 3 \times 3$ voxels. Filtering is performed every 5 iterations of the optimiser, and each time the deformation field is filtered 10 times.

All experiments were performed with the software package `elastix`,[13] developed by the authors. This registration package is largely based on the Insight Segmentation and Registration Toolkit.[14]
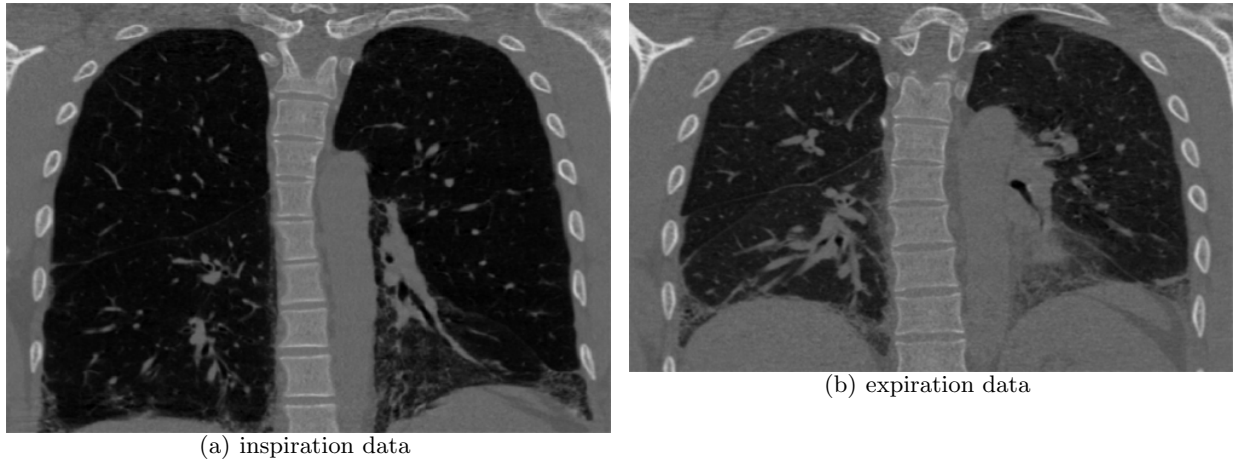
(a) inspiration data

(b) expiration data

Figure 2. Two coronal slices from CT data.

4.1. 2D synthetic example

We constructed a 2D synthetic example image to demonstrate the working of the registration with filtering compared to B-spline only registration. Figures 3(a) and 3(b) show the fixed and moving image, respectively, both with size 128×128. The central white structure represents a rigid structure, which creates the stiffness coefficient image, and the two other big white structures some other nonrigid image content. A standard B-spline registration was used with three resolutions, and in each resolution 50 iterations were performed. As said, a multigrid approach is taken. The B-spline grid spacing at the final resolution was set to 32 voxels. No affine or rigid registration is performed prior to nonrigid registration for the 2D synthetic images. The result of the B-spline registration is shown in Figure 3(c). From the difference image 3(d) it can be seen that the rigid inner structure has thickened. Clearly the B-spline fails to keep the inner rigid structure rigid, because the control points are pulled apart by the two big white structures moving outwards. The final deformation field resulting from the B-spline registration is adaptively filtered with the stiffness coefficient image, and applied to the moving image, resulting in Figure 3(e). The adaptive filtering compensates for the thickening of the inner rigid structure, maintaining the rigidity of the central structure. From the difference image in Figure 3(f) we see the inner structure mapping precisely onto itself in the fixed image.

4.2. 3D CT results

In Figure 4 surface renderings of the inspiration and expiration data of a patient are shown. All surface renderings are computed at a threshold of 150 Houndsfield Units (HU). To improve visualisations, small high intensity structures were removed.

Three resolutions were used for both registration algorithms. In each resolution we performed 300 iterations. The number of random samples used were 5000, 10000 and 20000, from the lowest to the highest resolution. B-spline grid spacings at the final resolution of both 32 and 16 voxels were explored. Prior to the nonrigid registration, an affine registration is performed in order to retrieve the global transformation. Voxels that do not lie within the cylindrically shaped CT beam were ignored.

The coefficient image c for the 3D CT data is created by thresholding the CT data at 150 HU, after which the intensities are rescaled between 0 and 1. This way we get a binary segmentation of the CT data: bone and other tissue.

Figure 5 displays typical results of registration both with and without adaptive filtering. Because of the large movement of the lungs in the vertical direction the B-spline control points are pulled downwards, and this results in a thickening of the ribs, see Figure 5(b). When the deformation field is filtered every 5 iterations, the thickening can be compensated for, see Figure 5(c). The original thickness of the rib is preserved, in contrast with standard B-spline registration results.
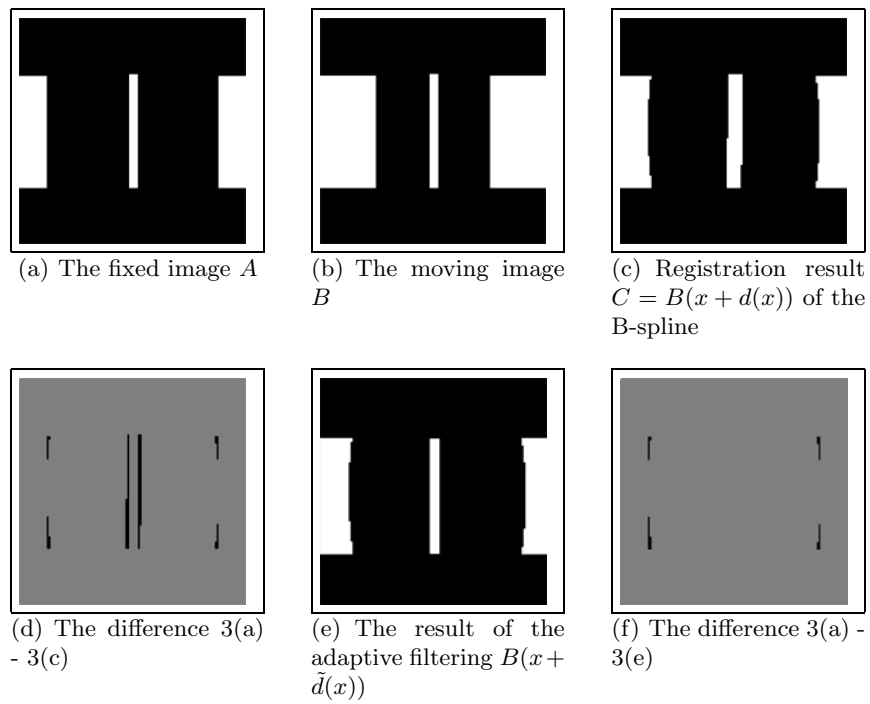
(a) The fixed image A

(b) The moving image B

(c) Registration result $C = B(x + d(x))$ of the B-spline

(d) The difference 3(a) - 3(c)

(e) The result of the adaptive filtering $B(x + \tilde{d}(x))$

(f) The difference 3(a) - 3(e)

Figure 3. Standard B-spline nonrigid registration compared with the adaptive filtering of the deformation field. The central white structure (3(a), 3(b)) represents rigid tissue, like bone. The central structure is deformed by the two other big nonrigid structures in the image.

(a) inspiration data
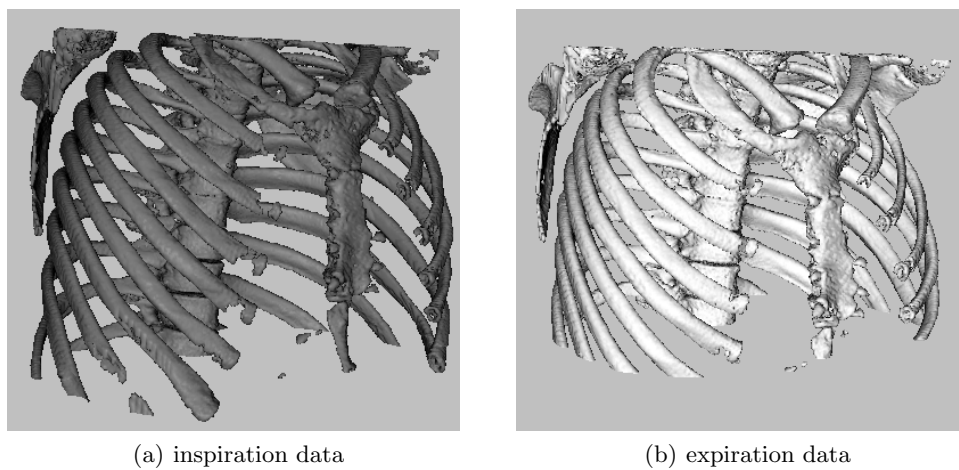
(b) expiration data

Figure 4. Surface renderings of a patient, showing the bony anatomy.

(a) inspiration data   (b) standard B-spline   (c) B-spline with adaptive filtering
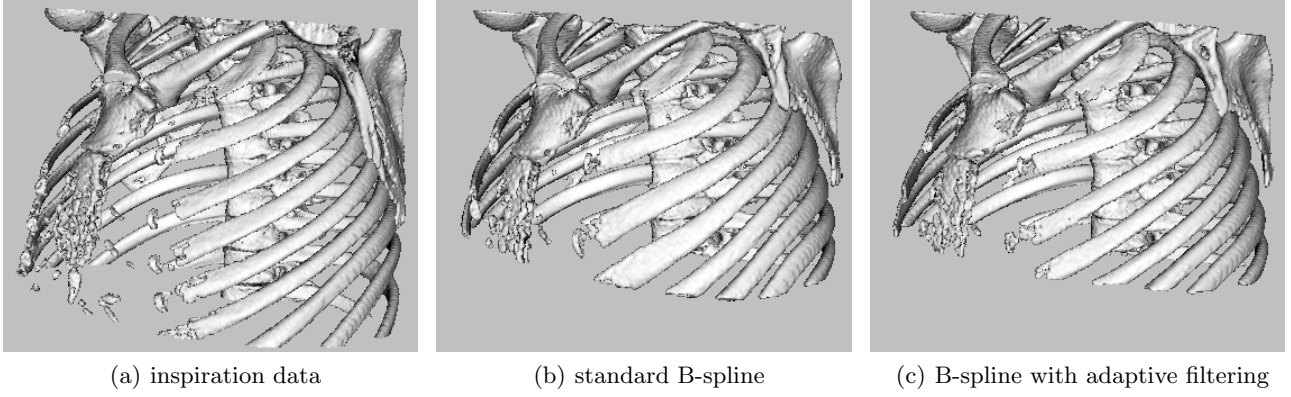
Figure 5. Surface renderings of patient data, showing the bony anatomy. The B-spline registration of inspiration-expiration data clearly distorts the rigidity of the ribs. The B-spline registration with adaptive filtering compensates for this effect.
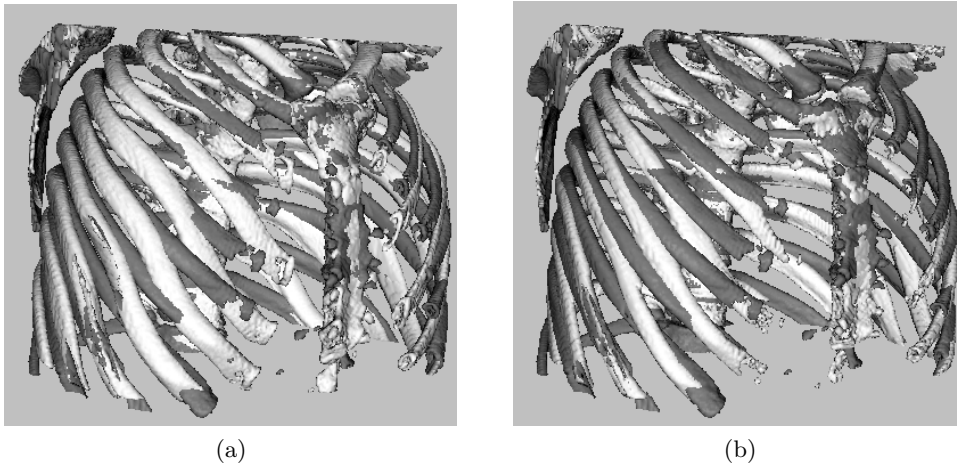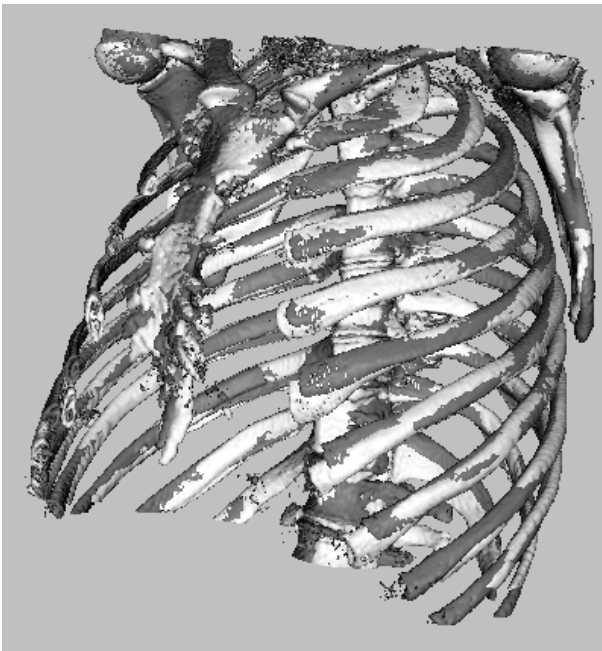

(a)   (b)

Figure 6. Surface renderings of patient data, showing the bony anatomy. The effect of a poor initialisation is shown. The inspiration data is shown in dark grey, and the result from B-spline registration without (a) and with adaptive filtering (b) in white.

For the nonrigid registration to work properly, a good initialisation provided by the affine registration is important. For two patients the overlap of the bones after the affine registration is insufficient; some ribs partly overlap with non-corresponding ribs. The B-spline registration will converge to an incorrect solution, thereby causing a nonrigid deformation of the ribs, as can be seen in Figure 6(a) and 6(b). With its limited extent, the adaptive filtering cannot compensate for the extensive bending of the ribs, although it does prevent the thickening of the ribs, thus improving the overlap of the ribs.

For the two other patients the affine registration is sufficient. After a B-spline registration all ribs overlap the right ribs as can be seen in Figure 7 for one of those patients. From Figure 7(a) and 7(b) it can be noticed that the overlap of the ribs increases using the adaptive filtering, getting a better and realistic registration. As can be seen from Figure 8, general registration quality improves.

In order to quantitatively evaluate the results of the adaptive filtering, the overlap of the bones of the inspiration image with the registered expiration image was calculated. The overlap measure is defined as

$$\text{overlap} \triangleq \frac{2 \cdot |V_1 \cap V_2|}{|V_1| + |V_2|}, \tag{9}$$
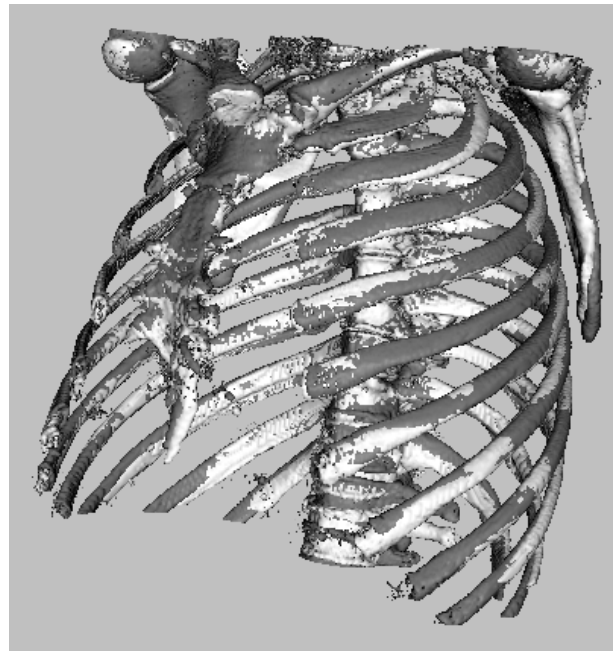
(a) (b)

Figure 7. Surface renderings of patient data, showing the bony anatomy. The inspiration data is shown in dark grey, and the result from B-spline registration without (a) and with adaptive filtering (b) in white. With a good initialisation corresponding ribs overlap. The adaptive filtering compensates for the thickening introduced by the B-splines, giving a better registration result.
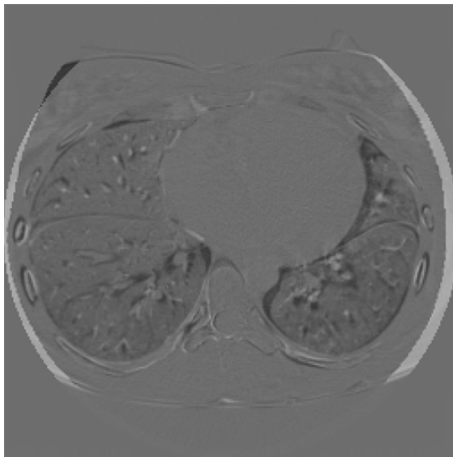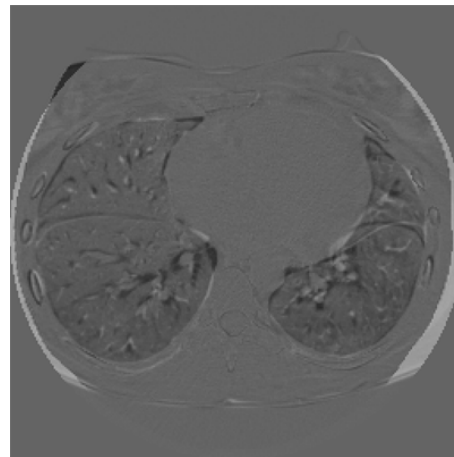
(a) standard B-spline registration (b) registration with adaptive filtering

Figure 8. A slice from the difference image between the inspiration data and the registered expiration data. Structures overlap better using adaptive filtering. Notice the improvement at the ribs and especially at the spine and shoulder blade. The lungs also show some improvement in overlap.
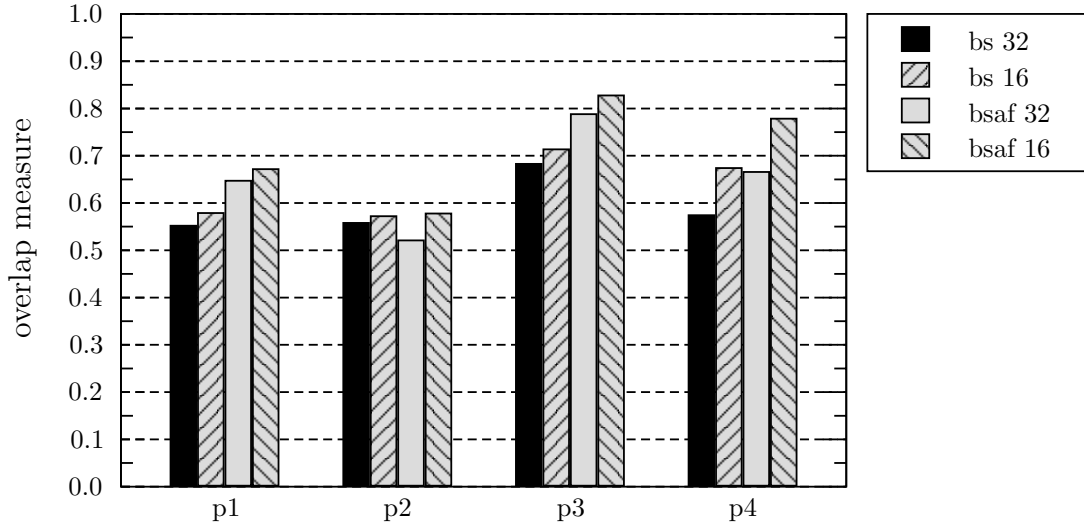
Figure 9. Overlap measures for the four patients, for the different registration methods. The abbreviations 'bs' and 'bsaf' refer to standard B-spline registration and B-spline registration with adaptive filtering, respectively. The numbers 16 and 32 refer to the final B-spline grid spacing used.

where V_i is the set of all voxels from bony structures, i.e. having an intensity higher than 150 HU. $|V_i|$ is the size of set V_i.

In Figure 9 the overlap measures for the four patients are shown. It can be seen that the overlap measure of the rigid tissue increases, when the grid spacing of the B-spline decreases. A denser B-spline grid is better suited to represent the real-world deformation.

In case of a poor initialisation (the first two patients) non-corresponding ribs overlap. In this case the overlap measure of Equation (9) makes less sense. Nevertheless, except for 'bsaf 32' compared to 'bs 32' for patient 2, the overlap measure increases. The surface renderings in Figure 6 confirm the overlap increase due to the compensation of the thickening by the adaptive filtering.

Provided a good initial registration is available (the latter two patients) the overlap measure increases substantially due to the adaptive filtering.

5. CONCLUSIONS AND DISCUSSION

In a standard B-spline based approach rigid tissue is deformed elastically. We propose a method that takes the rigidity of different tissue types into account, by an adaptive filtering of the deformation field.

Based on both visual inspection of the data, and the increase of overlap of bony structure, we conclude that the adaptive filtering of the deformation field is indeed able to improve registration results. Using the proposed registration gives anatomically more correct results by decreasing thickening and slight bending of rigid structures.

However, a good initial affine registration is required. In order to prevent a rib from bending, the filter could be applied even more times in succession than the 10 times we used here. As discussed in Section 2.1, the extent of the adaptive filter is then increased to a larger part of a rib. Secondly, improvement of the initial registration is an important step for further research, because, as can be noticed, final results depend heavily on this.

Because the adaptive filter is based on a weighted mean, the filtered deformation field will eventually evolve to a translational field, not allowing rotations of rigid objects. Future research will focus on developing a filter that yields a true rigid deformation field, allowing rotations in rigid parts.

REFERENCES

1. D. Rueckert, L. I. Sonoda, C. Hayes, D. L. G. Hill, M. O. Leach, and D. J. Hawkes, "Nonrigid registration using free-form deformations: Application to breast MR images," *IEEE Transactions on Medical Imaging* **18**(8), pp. 712 – 721, 1999.
2. J. P. Thirion, "Image matching as a diffusion process: an analogy with Maxwell's demons," *Medical Image Analysis* **2**(3), pp. 243 – 260, 1998.
3. P. Cachier, X. Pennec, and N. Ayache, "Fast non-rigid matching by gradient descent: Study and improvements of the demons algorithm," Research Report 3706, INRIA, 1999.
4. R. Stefanescu, X. Pennec, and N. Ayache, "Grid enabled non-rigid registration with a dense transformation and a priori information," in *Medical Image Computing and Computer-Assisted Intervention (MICCAI)*, *LNCS* **2879**, pp. 804 – 811, 2003.
5. P. J. Edwards, D. L. G. Hill, J. A. Little, and D. J. Hawkes, "A three-component deformation model for image-guided surgery," *Medical Image Analysis* **2**(4), pp. 355 – 367, 1998.
6. T. Rohlfing, C. R. Maurer, D. A. Bluemke, and M. A. Jacobs, "Volume-preserving nonrigid registration of mr breast images using free-form deformation with an incompressibility constraint," *IEEE Transactions on Medical Imaging* **22**(6), pp. 730 – 741, 2003.
7. P. Perona and J. Malik, "Scale-space and edge detection using anisotropic diffusion," *IEEE Transactions on Pattern Analysis and Machine Intelligence* **12**(7), pp. 629 – 639, 1990.
8. B. ter Haar Romeny, ed., *Geometry-Driven Diffusion in Computer Vision*, vol. 1, Kluwer Academic Publishers, 1994.
9. D. Mattes, D. R. Haynor, H. Vesselle, T. K. Lewellen, and W. Eubank, "PET-CT image registration in the chest using free-form deformations," *IEEE Transactions on Medical Imaging* **22**(1), pp. 120–128, 2003.
10. S. Klein, M. Staring, and J. P. W. Pluim, "Comparison of gradient approximation techniques for optimisation of mutual information in nonrigid registration," in *SPIE Medical Imaging: Image Processing*, (San Diego, California), 2005.
11. P. Thévenaz and M. Unser, "Optimization of mutual information for multiresolution image registration," *IEEE Transactions on Image Processing* **9**(12), pp. 2083 – 2099, 2000.
12. H. Lester and S. R. Arridge, "A survey of hierarchical non-linear medical image registration," *Pattern Recognition* **32**(1), pp. 129 – 149, 1999.
13. S. Klein and M. Staring, "`elastix`." `http://www.isi.uu.nl/Elastix/`.
14. "The Insight Segmentation and Registration Toolkit," `http://www.itk.org`.